Shear Strength of Fiber Reinforced Reactive Powder Concrete I-Shaped Beam without Stirrup

Ling-Zhi Jin[1], Xuan Chen[2], Feng Fu[3], Xiao-Fang Deng[4], and Kai Qian[5]

ABSTRACT

Due to the high compressive strength of steel fiber reinforced (SFR) and Reactive Powder concrete (RPC), higher degree of prestressing is available for the beams using fiber reinforced reactive powder concrete. Hence, a slenderer structural component can be designed, which could save self-weight, work spacing, and potential reducing the costs. However, comparing to conventional reinforced concrete (RC) beams, studies on post-tensioning SFR-RPC beams subjected to shear failure are fewer. In this study, a series of shear tests for four large-scale beams (one SFR-RPC beam and three post-tensioning SFR-RPC beams) are made to quantify the effects of levels of prestressing on shear load capacity of SFR-RPC beams. Finally, the test results together with data published from existing literatures are compared to the design strength calculated in accordance to different standards. It is found that the current code provisions will underestimate the shear load capacity significantly. In addition, an analytical model is proposed to predict the shear load capacity of the test specimens. A good correlation is observed with a mean analytical model to experimental strength ratio of 1.02 and coefficient of variation of 0.12.

CE Database subject heading: Shear Load Capacity, Beam, Post-Tension, Fiber Reinforced, Reactive Powder Concrete

---

[1] Professor, College of Civil Engineering and Architecture, Guilin University of Technology, Guilin, China, 541004

[2] Research Student, College of Civil Engineering and Architecture, Guilin University of Aerospace Technology, Guilin, China, 541004

[3] Senior Lecturer, Department of Civil Engineering, City, University of London, London, EC1V 0HB, U.K.

[4] Assistant Professor, College of Civil Engineering and Architecture, Guilin University of Technology, Guilin, China, 541004

[5] Professor, College of Civil Engineering and Architecture, Guangxi University, China, 541004

(Corresponding author), qiankai@ntu.edu.sg

INTRODUCTION

Reactive powder concrete (RPC), which was first developed in the mid-1990s by the Bouygues' laboratory in France (Richard and Cheyrezy 1994), has attracted considerable attentions from engineering and academic communities due to its excellent mechanical performance. The studies on material behavior (Farhat et al. 2007, Graybeal and Tanesi 2007, Yoo et al. 2014, and Li and Liu 2016) had indicated that structural components built by RPC exhibited better durability, energy dissipation capacity, and fatigue behavior comparing to conventional concrete materials. Moreover, due to its higher compressive strength , it is more suitable for prestressed concrete which could further reduce the weight of the structural components and subsequently, the costs. Thus, RPC has been widely used in bridge engineering, i. e. Sherbrooke Pedestrian Bridge with 60 m span crossing the river of Magog in Canada; the Seonyu Bridge with an arch spanning 120 m etc. (Voo et al. 2006).

In the past decade, extensive studies had been carried out on application of RPC materials in modern structures, not only on enhancing the mechanical properties of RPC. Extensive studies (Graybeal 2008, Chen and Graybeal 2012, Yang et al. 2010, Yoo and Yoon 2015, Dancygier and Berkover 2016, Chen et al. 2018, Lu and Chu 2019, Kotsovos and Zygouris 2019, Yang et al. 2019, Azam et al. 2019, and Mun and Yang 2019) had been carried out to investigate the flexural behavior of reactive powder concrete (RPC) beams with or without prestressing strands. However, comparing to flexural behavior of RPC beams, studies on shear load capacity of RPC beams are few. Voo et al. (2006) tested seven prestressed I-shaped RPC girders without stirrups. The variables investigated are types and amount of fibers in RPC mix. It is concluded that the type and amount of fibers has little effects on the initial shear cracking load but increasing the fiber volume will enhance the shear load capacity significantly. Ji et al. (2018) tested twelve T-shaped girders to study the

influence of shear span-to-depth ratio, longitudinal reinforcement ratio, and stirrups ratio on the shear load capacity and failure mode. Moreover, an improved softened truss model is developed based on test results. However, it should be pointed out that few studies had been carried out on quantifying the impact of degrees of prestressing on shear load capacity of RPC I-shaped beams. Therefore, in this paper, one SFR-RPC beam and three post-tensioning SFR-RPC beams are tested for above purpose. The ultimate load on inclined plane , width of inclined crack, deflection and failure pattern of the test beams are investigated. Moreover, based on test results, the reliability of existing design equations for shear load capacity of RPC is evaluated. Furthermore, analytical models are derived to predict the shear capacity of post-tensioning RPC I-shaped beams.

RESEARCH SIGNIFICANCE

The primary objective of this paper is to experimentally evaluate the shear load capacity of post-tensioned RPC T-shaped beams with various effective prestress. The significance of the test lies in the fact that such large-size tests of post-tensioned T-shaped RPC beams, which are more representative of the complex mechanisms in real RPC beams, are rare in literature. Moreover, the test results may help researchers and design engineers to understand the effects of effective prestress in RPC beams subjected to shear test. Furthermore, the findings from this study may provide evidence to establish more convincing design guidelines, the reliability of design equations from main standards or codes is evaluated and a semi-analytical model is proposed.

DESCRIPTION OF TEST PROGRAM

Test Specimens

As aforementioned, seven SFR-UHPC beams with different level of prestress force were loaded monotonic until failure to investigate the contribution from each component of the beam to shear capacity and to quantify the effects of level of prestress on shear behavior of SFR-UHPC I-shaped beams. Fig. 1 shows

the dimensions and reinforcement details of test specimens, while Table 1 tabulates the main characteristic of test specimens. The specimens are denoted as follows: PC-2.0-0.46 represents post-tensioning specimen with shear span-to-depth ratio of 2.0 and level of prestress of 0.46 while RPC-2.0-0.0 means non-prestressed RPC beam with shear span-to-depth ratio of 2.0. As shown in Fig. 1, the beams have a total length of 2.6 m and a single span of 2.0 m. The height of the beam is 400 mm, with a web thickness of 70 mm and flanges width of 200 mm. For Specimen RPC-2.0-0.0, the flange is reinforced by 3Φ25. However, the flange of PC specimens is reinforced 2Φ25. The yield strength and ultimate strength of Φ25 is 548 MPa and 728 MPa, respectively. For post-tensioning specimens, 2Φ15.2 strands are designed. The ultimate strength and nominal area of Φ15.2 strand is 1860 MPa and 139 mm^2, respectively.

Material Properties

Table 2 gives the SFR-RPC mixes in detail. The SFR-RPC used in this study is produced by a high energy concrete mixer. The mix proportions of SFR-RPC are: cement (c) equals to 872 kg/m^3, silica fume (SF) equals to 262 kg/m^3, coarse quartz sand (0.6 mm to 1.25mm) equals to 174 kg/m^3, medium quartz sand (0.3 mm to 0.6 mm) equals to 698 kg/m^3, fine quartz sand (0.16 mm to 0.32mm) equals to 174 kg/m^3, water (W) equals to 200 kg, superplasticizer (Sup) equals to 17 kg. Straight fiber with length ranged between 12 mm to 15 mm, and diameter of 0.2 mm is used in this study. The designed tensile strength of the steel fiber is 2000 MPa. All beams have dosage of steel fiber of 0.75 % (volume) and about 60 kg/m^3. The mix proportion is identical for all RPC specimens; however, natural and steam curing conditions were considered in the test. The temperature of natural curing is from 30 to 40˚c and with covered and watering to 28 days.

The results of the material for test specimens are summarized in Table 3. The mean compressive strength (f_{cm}) is measured by six 100×100×300 mm prism using load control method with a rate of 1.3 MPa/s. The modulus (E_0) and Poisson's ratio (υ) are also measured as the stress-strain curve is measured when we test the 100×100×300 mm prisms. The cube compressive strength (f_{cu}) was obtained from 100 mm cubes stressed

under load control at a rate of 1.3 MPa/s. The cubic tensile splitting strength (f_t) is obtained from tests on six 100 mm cubes at a rate of 0.2 MPa/s. Then, the flexural tensile strength (f_{tm}) is measured from 100 mm square prisms spanning 400 mm with a notch depth of 25 mm.

Test Setup

Fig. 2 shows the setup and instrumentation layout in detail. The dimension of the bearing plate is 200 mm×100mm while the dimension the loading plate is 300 mm×80mm. Before testing, the strands were post-tensioned with allowance of the prestress losses. As the specimens were tested 15 mins after prestressing, the loss due to anchorage can be considered as Eq. 1.

$$\sigma_{l1} = \frac{a}{l} E_{ps} \tag{1}$$

where σ_{l1} is the loss due to anchorage; a is the gap of anchorage (3 mm is assumed); l is the length of the beam (2600 mm); E_{Ps} is the elastic modulus of the strands.

Therefore, the applied prestressing stress for Specimens PC-2.0-0.46, PC-2.0-0.65, and PC-2.0-0.3 are 1077 MPa, 1477 MPa, and 777 MPa, respectively. After prestress force loss, the measured average effective prestressing stress in the two strands of Specimens PC-2.0-0.46, PC-2.0-0.65, and PC-2.0-0.3 are 863 MPa, 1244 MPa, and 570MPa, respectively.

As shown in Fig. 2, simple supported SFR-RPC beams were tested under asymmetric three-point bending setup as shear behavior of test specimens was the main concern (Voo et al. 2010, Meszoly and Randl 2018). All beams had a total length of 2.6 m and a single span of 2.0 m. As shown in Fig. 2, linear variable displacement transducers (LVDT) were installed at the position of the supports to monitor the movement of the supports during tests. Moreover, LVDTs were also installed underneath the loading point, middle span, and one-quarter span of the beam to measure the deflections. A series of strain gauge rosettes were attached

to obtain the principal strain direction. At the section of loading point, a series of concrete gauges were installed parallel to monitor the strain distribution. Strain gauges were also attached along the longitudinal reinforcement.

EXPERIMENTAL RESULTS

Global Behavior

Non-prestressed Specimen RPC-2.0-0.0 — Fig. 3 shows the load-displacement curve of test specimens. When the vertical load reached 83 kN, flexural crack was first observed at the bottom flange of the beam, which was 80 mm distance from left support. The width of the crack was less than 0.01 mm. At a load of 99 kN, first diagonal crack occurred at the web of the beam, which was 400 mm from left support. The angle of the diagonal crack was about 49 degrees and the crack width was only 0.02 mm. Further increase of the load to 128 kN, more diagonal cracks were also observed at the web nearby the right support with maximum width of 0.04 mm. When the load reaching 160 kN, more diagonal cracks occurred at the web nearby the left support. And these diagonal cracks were developed towards the loading point and left support. When the load reached 279 kN, those small diagonal cracks were developed into a large diagonal crack with maximum width of 0.82 mm. Moreover, vertical cracks formed along the interface between the top flange and the web at this loading stage. The width of diagonal crack increased to 1.25 mm at a load of 318 kN. Sounds due to fracture of steel fibers occurred continuously when further increase of the load. The main diagonal crack suddenly opened up at a load of 345 kN and test was stopped. The failure mode of this specimen is shown in Fig. 4. As shown in the figure, the inclination angle between the main diagonal crack and beam axis is 39 degrees.

Prestressed Specimen PC-2.0-0.3— This specimen was prestressed with a controlling stress of $0.3f_{su}$. f_{su} was the ultimate strength of strands (1860 MPa). The first flexural crack occurred at a load of 138 kN, which was 166 % of that of RPC-2.0-0.0, at a distance of 70 mm away from left support. The width and length

of the flexural crack was 0.01 mm and 80 mm, respectively. Then, when the load reached 178 kN, the first diagonal crack with inclination angle of 37 degrees formed in the web. The width of the crack was about 0.11 mm. Further increasing the load to 185 kN, more diagonal shear cracks formed at the short span side. When the load reached 268 kN, 8 diagonal shear cracks were observed in the left side and the maximum crack width was 0.59 mm. After that, more cracks occurred in the beams including flexural and shear cracks and the cracks were developed and connected. Two main diagonal cracks with width of 0.76 mm formed in left side at a load of 304 kN. Further increasing the load, no new cracks formed but the width of the cracks kept increasing. At a load of 364 kN, which was 106 % of that of RPC-2.0-0.0, the diagonal shear crack suddenly opened with a maximum width of 1.5 mm. The specimen was failed and test was stopped. Fig. 5 shows the failure mode of the Specimen PC-2.0-0.3.

Prestressed Specimen PC-2.0-0.46— This specimen was prestressed with controlling stress of $0.46f_{su}$. Different to PC-2.0-0.3, the first crack formed in PC-2.0-0.46 was a diagonal shear crack at a load of 213 kN, rather than flexural crack. The diagonal shear crack formed in the web with an inclination angle of 36 degrees. After that, flexural cracks formed at the bottom flange in the left span. When the load reached 258 kN, diagonal crack was also observed in the web of right span. The 0.53 mm wide diagonal shear crack in the left side were developed at a load of 348 kN, the diagonal shear crack in the left side became much wider and extended into the left support. At this stage, a number of flexural-shear cracks formed in the right span. The width of main diagonal shear crack in the left side reached 1.6 mm and sounds due to fracture of steel fiber occurring continuous at a load of 370 kN. The ultimate load of 390 kN was obtained at a vertical displacement of 5.5 mm. The failure mode of this specimen is illustrated in Fig. 6.

Prestressed Specimen PC-2.0-0.65— This specimen is prestressed with controlling stress of $0.65f_{su}$. Similar to PC-2.0-0.46, the first crack in PC-2.0-0.65 is diagonal shear crack at a load of 290 kN. The diagonal shear crack is formed in the web with an inclination of 31 degrees and the crack width is less than 0.11. At a

load of 370 kN, more diagonal cracks with maximum width of 0.13 mm formed in the left shear span. And no diagonal cracks were observed in the right shear span at this loading stage. Then, further increasing the load to 388 kN, cracks were observed along the interface of top flange and web. At a load of 450 kN, three parallel diagonal shear cracks were formed in the left shear span with maximum crack width of 0.76 mm. The ultimate load capacity of 487 kN was reached at a vertical displacement of 4.6 mm (beneath the loading point). The failure mode of Specimen PC-2.0-0.65 is shown in Fig. 7.

Strain Gauge Readings

Fig. 8 illustrates the strain gauge readings on the longitudinal reinforcement of the beam. The location of the strain gauges is shown in Fig. 9. As shown in Fig. 8, it is found that the maximum strain reading was less than 2500 με for all beams that represented, and no longitudinal reinforcement yielded. For Specimen RPC-2.0-0.0, Z5 and Z6 achieved the maximum tensile strain as these strain gauges were mounted close to the loading point. Moreover, considerable tensile strain was measured at Z1, which was mounted at the left support, after severe diagonal shear crack occurred in the web. This means the dowel action of longitudinal reinforcement could provide certain shear resistance. For prestressed specimens PC-2.0-0.3, PC-2.0-0.46, and PC-2.0-0.65, considerable compressive strain was obtained initially due to prestress force, especially for PC-2.0-0.65. Similar to RPC-2.0-0.0, the tensile strain increased faster after shear failure occurred in the web. However, post-tensioning strands had minimal effects on the maximum tensile strain of the beam longitudinal reinforcement.

Load-Crack Width Curve and Stress in Strands

Fig. 10 illustrates the relationship between applied load and crack width. As shown in the figure, the first diagonal crack was observed in the web of Specimen RPC-2.0-0.0, PC-2.0-0.3, PC-2.0-0.46, and PC-2.0-0.65 at the loads of 99 kN, 178 kN, 213 kN, and 290 kN, respectively. Therefore, it can be concluded using the

post-tensioning strands can increase the crack load up 193.0 %. Consequently, the maximum width of Specimen RPC-2.0-0.0, PC-2.0-0.3, PC-2.0-0.46, and PC-2.0-0.65 is 1.9 mm, 1.6 mm, 1.5 mm, and 1.0 mm, respectively. Therefore, the post-tensioning strands with controlling stress of $0.65f_u$ could reduce the width of the diagonal shear crack by 47.4 %.

Fig. 11 gives the change of stress in post-tensioning strands of PC specimens. It can be seen that, the stress in strands is linearly increased with the increase of the displacement at the loading point. The increment of stress in strands for PC-2.0-0.3, PC-2.0-0.46, and PC-2.0-0.65 are only 91 MPa, 91 MPa, and 72 MPa, respectively. Therefore, comparing to the initial stress in strands, the increment is negligible. This could be explained as the three-point loading method led to much less deformation capacity of the beam.

ANALYTICAL ANALYSIS AND DISCUSSION

Comparison of the Ultimate Load from Major design Codes and Test Results

To evaluate the reliability of existing codes for predicting the ultimate load of T-shaped SFR-RPC beams without stirrups, the ultimate load measured from test andsimilar specimens from literature was compared with the analytical values from the classic codes, such as ACI 318-08 (2008), JSCE (2006), and AFGC (2013). As all specimens were designed without stirrups, the contribution of stirrups was not included in their formulas.

ACI 318-08 (2008):

$$V_{u,ACI} = (0.29\sqrt{f_{cm}} + 0.3 f_{pc})bd + V_p \quad (2)$$

where f_{cm} is concrete cylinder strength; b is width of web; d is beam effective depth, V_p is vertical component of effective prestress force.

AFGC (2013):

$$V_{u,AFGC} = \frac{0.24}{\gamma_{cf}\gamma_E}\sqrt{f_{cm}}bd + \frac{bz\sigma_{Rd.f}}{\tan\theta} \quad (3)$$

where $\gamma_{cf}\gamma_E$ is a structural safety factor; z is the length of internal force arm; $\sigma_{Rd,f}$ is the residual tensile strength of UHPC fiber; θ is the angle between principal compressive stress and beam axis.

JSCE (2006):

$$V_{u,JSCE} = \frac{0.18}{\gamma_b}\sqrt{f_{cm}}bd + \frac{f_{vd}bz}{\gamma_b \tan\beta_u} + \frac{P_e \sin\beta}{\gamma_b} \quad (4)$$

where γ_b is a component safety factor; f_{vd} is design tensile strength of UHPC at shear diagonal cracks; β_u is the angle between diagonal crack and beam axis; P_e is effective prestress force; β is the angle between prestressed tendon and beam axis.

Table 5 compares the analytical results with the test ones. As shown in the table, the formulas proposed from ACI 318-08 (2008), and JSCE (2006), and AFGC (2013) underestimate

the ultimate load capacity for various reasons. For ACI 318-08 (2008), and JSCE (2006), the lower estimation mainly due to the ignorance of the contribution of fibers and the arch action due to short shear-span/depth ratio. Although AFGC (2013) achieved best prediction, it overlooks of the effects of prestressing forces and arch action resulting too conservative results. Therefore, to give a commonly accepted formula for prediction of shear load capacity of SFR-RPC beams, a semi-empirical model is proposed by including the effects of prestressing force and arch action due to relatively lower shear-span/depth ratio.

Analytical model for shear load capacity

Similar to conventional reinforced concrete beams, the effects of shear span ratio, concrete strength, longitudinal reinforcement ratio, volume of steel fibers, and dimensions of the beams on the shear load

capacity of SFR-RPC should be incorporated into the proposed formula. Similar to existing codes (such as AFGC 2013), the formula is expressed as the superposition of the concrete term and prestressing force term., which can be written as Eq. 5.

$$V_u = V_c + V_p \tag{5}$$

The first term V_c in Eq. 5 is the concrete term, which considers the effects of shear span ratio, longitudinal reinforcement ratio, and volume of steel fiber. As the shear capacity of RPC beams decreases with the increase of shear-span ratio, the shear load capacity of the RPC beam is proportional to $\frac{1}{\lambda}$. Thus, for generalization, the effects of shear span ratio are expressed as Eq. 6.

$$K_\lambda = \frac{k_1}{(\lambda + k_2)} \tag{6}$$

where λ is the shear span ratio, k_1 and k_2 are the constants, K_λ is a influencing factor for shear span ratio.

Moreover, the effects of the longitudinal reinforcement ratio should be considered as the feature of RPC and steel fibers in RPC could ensure the longitudinal reinforcement to contribute shear resistance by dowel action, which is related to the ratio of longitudinal reinforcement ratio to compressive strength of concrete. Therefore, based on correlation analysis, the effects of shear span ratio and longitudinal reinforcement ratio could be expressed as:

$$\frac{V_c^{'}}{f_{cm} bd} = K_\lambda + K_\rho \frac{\rho}{f_{cm}} \tag{7}$$

where $\frac{\rho}{f_{cm}}$ represents the characteristic of the longitudinal reinforcement ratio, K_ρ is an influencing factor for longitudinal reinforcement ratio.

Furthermore, as the steel fibers could partially maintain the residual strength even the cracks were formed, the effects of steel fiber are considered by an increasing factor $1+\beta_v v_f$.

where β_v is an influencing factor of steel fiber, which could be obtained by Table 6, v_f is the volume ratio of the steel fiber.

Thus, the concrete term is expressed as $V_c = V_c^{'}(1+\beta_v v_f)$.

As mentioned above, existing design equations proposed in ACI 318-08 (2008), JSCE (2006), and AFGC (2013) did not take into account the difference of arch action for short beams and beam action for slender beams. Therefore, as suggested by Rebeiz (1999), an interpolation function is proposed to account to effects of arch action. Thus, the concrete term is finally expressed as $V_c = V_c^{'}(1+\beta_v v_f)(k_3 + k_4 A_d)$.

where k_3 and k_4 are the constants, A_d is shape adjustment factor($A_d = \lambda$ for $1.0 < \lambda < 2.5$, $A_d = 2.5$ for $\lambda \geqslant 2.5$), similar to Rebeiz (1999).

For the term of prestressing force V_p, as the effective prestressing force could delay the forming of cracks and increase the compression zone of the concrete, the enhancement factor is expressed as:

$$V_p = k_3 N_{p0} \tag{8}$$

where N_{p0} is the effective prestressing force.

Based on regression analysis, the factors of k_1, k_2, and k_3 were determined and the formula for no stirrups SFR-RPC T beams with prestressing strands were expressed as:

$$V_u = \left(\frac{0.070}{\lambda - 0.852} + \frac{49.086\rho}{f_{cm}}\right) f_{cm} bd(1 + \beta_v v_f)(0.755 + 0.054A_d) + 0.258N_{p0} \quad (9)$$

Comparison of the Predicted Ultimate Loads from the Proposed Formula and the Test Results

Table 6 and Fig. 12 show the comparison of the ultimate load predicted from proposed formula and that from the test results of literatures of RPC beams without stirrups. As shown in the table, in general, the ratio of predicted load to tested counterpart has mean value of 0.998 and standard deviation of 0.129. Thus, the proposed formula could predict the shear load capacity of the RPC beams with convention or steel fiber reinforced concrete with high level of confidence. To evaluate the accuracy of proposed formula for special parameters, the comparison of theoretical values of the shear load capacity from Eq. 9 with the experimental value obtained from tests is shown in Fig. 12. For special parameters, the model works well for shear span/depth ratio ranged from 1.2 to 4.5. For prestressing force at bottom flange ranged from 200 kN to 900 kN and beam longitudinal reinforcement ratio ranged from 1.5% to 3.0%, the model could give well prediction. However, the model could not give reasonable results for concrete cylinder strength less than 80 MPa or larger than 150 MPa.

CONCLUSIONS

Following conclusions can be made from the experimental study conducted in this study:

1. The prestressing force will not affects the shear failure mode of T-shaped RPC beams but have a significant influence on the initial stiffness, crack load capacity, crack propagation, and ultimate load capacity.

2. Because of the bridging effect from steel fiber, the formation and propagation of diagonal cracks are reduced.

3. The strain gauge results confirmed that the dowel action of longitudinal reinforcement could provide additional load resistance after diagonal crack occurred.

4. The prestressing force will affect the stress distribution of longitudinal reinforcements, but it has little effects on the maximum tensile strain.

5. The ultimate load obtained from the tests was compared to the one from typical standards or codes. It indicates that ACI 318-08 (2008) achieves much lower prediction as the contribution of prestressing force and steel fibers are ignored. However, the prediction of AFGC (2013) and JSCE (2006) are better off, although the contribution of prestressing force is also ignored.

6. Based on the test observations and analysis of the influencing factors, a semi-empirical analytical model is proposed for the T-shaped SFR-RPC beams without stirrups. By comparison of the prediction values with the test results, it could accurately predict the shear load capacity of the T-shaped SFR-RPC beams with stirrups generally. The proposed semi-empirical model could predict the shear load capacity of short beam with low shear-span/depth ratio and slender beam with large shear-span/depth ratio well. Moreover, the model predicts the shear load capacity of RPC beams with different prestressing force at bottom flange and longitudinal reinforcement ratio fairly well. However, the model is not suitable for the beams with normal concrete strength (less than 80 MPa).

REFERENCES

ACI Committee 318 (2008) Building code requirements for structural concrete (ACI 318-08) and commentary (318R-08). *American Concrete Institute*, Farmington Hills, MI, 503 pp.

AFGC. (2013) Ultra high performance fibre-reinforced concretes interim recommendations. AFGC-SETRA, Bagneux, France.

Azam R, Soudki K, West J, Noei M. (2019) CFRP grid embedded in mortar for strengthening of shear-critical RC beams. *Magazine of Concrete Research*, in press.

Baby F, Marchand P, Toutlemonde F (2014) Shear behavior of ultrahigh performance fiber-reinforced concrete beams. I . Experimental investigation. *Journal of Structural Engineering* ASCE, **140(5):**04013112.

Baby F, Marchand P, Toutlemonde F (2014) Shear behavior of ultrahigh performance fiber-reinforced concrete beams. II. Analysis and design provisions. *Journal of Structural Engineering* ASCE, **140(5)**:04013111.

Chen L, Craybeal B. (2012) Modeling structural performance of second-generation ultrahigh-performance concrete pi-girders. *Journal of Bridging Engineering* ASCE, **17(4)**:634-643.

Chen SM, Zhang R, Jia LJ, Wang JY. (2018) Flexural behavior of rebar-reinforced ultra-high-performance concrete beams. *Magazine of Concrete Research*, **70(19),** 997-1015.

Dancygier AD, Berkover E. (2016) Cracking localization and reduced ductility in fiber-reinforced concrete beams with low reinforcement ratios. *Engineering Structures*, **115(15)**:411-424.

Dinh H, Parra-Montesinos G,Wight JK. (2011) Shear strength model for steel fiber reinforced concrete beams without stirrup reinforcement. *Journal of Structural Engineering*, **137(10)**:1039-51.

Dupont D, Vandewalle L.(2003) Shear capacity of concrete beams containing longitudinalreinforcement and steel fibers. SP-216. *American Concrete Institute*, Farmington Hills (MI): 79-94.

Farhat FA, Nicolaides D, Kanellopoulos A, Karihaloo BL (2007) High performance fibre-reinforced cementitious composite (CARDIFRC)-performance and application to retrofitting. *Engineering Fracture Mechanics,* **74(1-2):** 151-167.

Graybeal B, Tanesi J (2007) Durability of an ultrahigh-performance concrete. *Journal of Materials in Civil Engineering*, **19(10):** 848-854.

Graybeal B (2008) Flexural behavior of an ultrahigh-performance concrete I-girder. *Journal of Bridge Engineering*, **13(6):** 602-610.

Japan Society of Civil Engineers (JSCE). (2006) Recommendations for design and construction of ultrahigh strength fiber reinforced concrete structures (Draft). *JSCE Guideline for Concrete No.9,* Tokyo.

Ji WY, Li WW, An MZ, Zhu L (2018) Shear capacity of T-Section girders made of reactive powder concrete. *Journal of Bridging Engineering* ASCE, **23(7)**:04018041.

Kotsovos GM, Zygouris, NS. (2019) RC frame analysis with mode of failure prediction capability. *Magazine of Concrete Research,* **71(3),** 109-125.

Kwak Y, Eberhard MO, Kim WS, Kim J. (2002) Shear strength of steel fiber-reinforced concrete beams without stirrups. *ACI Structural Journal,* **99(4):**530-8.

Li H, Liu G (2016) Tensile properties of hybrid fiber-reinforced reactive powder concrete after exposure to elevated temperatures. *International Journal of Concrete Structures and Materials,* **10(1):** 29-37.

Lim WY, Hong SG (2016) Shear tests for ultra-high performance fiber reinforced concrete (UHPFRC) beams with shear reinforcement. *International Journal of Concrete Structures and Materials*, **10(2):** 177-188.

Lu WY, Chu CH. (2019) Tests of high-strength concrete deep beams. *Magazine of Concrete Research,* **71(4),** 184-194.

Meszoly T, Randel N (2018) Shear behavior of fiber-reinforced ultra-high performance concrete beams. *Engineering Structures*, **168**: 119-127.

Mun JH, Yang KH. (2019) Flexural behavior of externally post-tensioned two-span lightweight concrete beams. *Magazine of Concrete Research*, in press.

Rebeiz K S . (1999) Shear strength prediction for concrete members. *Journal of Structural Engineering*, **125(3):**301-308.

Richard P, Cheyrezy M (1994) Reactive powder concretes with high ductility and 200-800 MPa compressive strength. *ACI, **SP-144(24)***, San Francisco, USA, 507-518.

Voo YL, Foster SJ, Gilbert RI (2006) Shear strength of fiber reinforced concrete reactive powder concrete prestressed girders without stirrups. *Journal of Advanced Concrete Technology*, **4(1):** 123-132.

Voo YL, Poon WK (2010) Shear strength of steel fiber-reinforced ultrahigh-performance concrete beams without stirrups. *Journal of Structural Engineering* ASCE, **136(11):**1393-400.

Wu X, Han SM (2009) First diagonal cracking and ultimate shear of I-shaped reinforced girders of ultra high performance fiber reinforced concrete without stirrups. *International Concrete Structures and Material*, **3(1):**47-56.

Yang H. (2014) Experimental study on shear behaviors of steel fiber reinforced full-lightweight concrete beams without web reinforcement. North China University of Water Resources and Electric Power, Henan, China.

Yang IH, Joh CB, Kim BS. (2010) Structural behavior of ultra high performance concrete beams subjected to bending. *Engineering Structures*, **32(1)**, 3478-3487.

Yang JM, Kim JK, Yoo DY. (2019) Flexural and shear behavior of high-strength SFRC beams without stirrups. *Magazine of Concrete Research*, in press.

Yoo DY, Shin HO, Yang JM, Yoon YS. (2014) Material and bond properties of ultra high performance fiber reinforced concrete with micro steel fibers. *Composites Part B: Engineering*, **58**, 122-133.

Yoo DY, Yoon YS. (2015) Structural performance of ultra-high-performance concrete beams with different steel fibers. *Engineering Structures*, **102**, 409-423.

Zhou JL. (2017) The study of prestressed RPC simply-supported with different shear span ratio shear capacity. *Guilin University of technology*, Guangxi, China.

FIGURE CAPTIONS

Figure 1. Dimensions and reinforcement detailing of test specimens: (a) non-prestressed specimen, (b) prestressed specimens

TABLE CAPTIONS

Table 1. Specimen properties

Test ID	Shear Span (mm)	Effective Depth (mm)	Targeted λ*	True λ	Amount of Strands	Amount of Longitudinal Rebar
RPC-2.0-0	700	350	N/A	N/A	N/A	3Φ15.2
PC-2.0-0.30	700	350	0.3	0.31	2Φ15.2	3Φ15.2
PC-2.0-0.46	700	350	0.46	0.46	2Φ15.2	3Φ15.2
PC-2.0-0.65	700	350	0.65	0.67	2Φ15.2	3Φ15.2

Note: λ* is defined as the effective controlling stress in strands

Table 2. Fiber reinforced RPC mix design (material quantities in kg per of m^3 RPC)

W/B	C/kg	SF/kg	CQ/kg	MQ/kg	FQ/kg	Water	Sup	Fiber
0.23	872	262	174	698	174	200	17	60

Note: RPC represents reactive powder concrete; C represents cement; SF represents silica fume; CQ represents coarse quartz sand with size ranged between 0.6 mm to 1.25 mm; MQ represents medium quartz sand with size ranged between 0.3 mm to 0.6 mm; FQ represents fine quartz sand with size ranged from 0.16 mm to 0.32 mm.

Table 3. Mechanical properties

Test ID	f_{cu} (MPa)	f_{cm} (MPa)	f_t (MPa)	f_{tm} (MPa)	E_c (GPa)	υ
RPC-2.0-0	119.2	106.5	5.8	17.8	41	0.2
PC-2.0-0.30	111.3	103.7	5.6	19.7	40	0.2
PC-2.0-0.46	117.8	105.7	5.8	19.8	41	0.2
PC-2.0-0.65	125.1	105.1	5.7	16.6	42	0.2

Table 4. Test results

Test ID	F_{cr} (kN)	Crack width (mm)	F_u (kN)	V_u (kN)
RPC-2.0-0	99.0	1.9	345	224.1
PC-2.0-0.30	178.0	1.6	364	236.9
PC-2.0-0.46	213.0	1.5	390	253.5
PC-2.0-0.65	290.0	1.0	487	316.4

Note: F_{cr} and F_u are the crack load and ultimate load, respectively; V_u is the shear load capacity.

Table 5. Comparison of test results with the values calculated by foreign codes

Reference	No.	Specimen	$V_{u,exp}$(kN)	$V_{u,ACI}/V_{u,exp}$	$V_{u,AFGC}/V_{u,exp}$	$V_{u,JSCE}/V_{u,exp}$
This study	1	RPC-2.0-0	224.1	0.33	0.65	0.52
	2	RPC-2.0-0.30	236.9	0.50	0.86	0.67
	3	RPC-2.0-0.46	253.5	0.57	0.82	0.64
	4	RPC-2.0-0.65	316.4	0.55	0.78	0.60
			Average	0.49	0.78	0.61
			COV	0.22	0.12	0.11

Note: $V_{u,exp}$ represents the measured ultimate shear load; $V_{u,ACI}$, $V_{u,AFGC}$, and $V_{u,JSCE}$ represent the predicted shear load capacity based on ACI 318-08 (2008), AFGF (2013), and JSCE (2006), respectively.

Table 6. The value of β_v

Types of fiber	Deformed	Milling	Cut by Steel Wire	Shear Flat
β_v	0.7	0.9	0.6	0.5

1

2

3

1

2 Table 7. Summary of beam specimens

Reference	No.	Specimen	f_{cm} (MPa)	b (mm)	d (mm)	a/d	ρ (%)	V_f (%)	β_v	$P_{e,bot}$ (kN)	$V_{u,\exp}$	$V_u/V_{u,\exp}$
This study	1	RPC-2.0-0	106.5	70	350	2	2.9	0.75	0.5	0	224.12	1.02
	2	RPC-2.0-0.30	103.7	70	350	2	1.9	0.75	0.5	216.0	236.86	1.07
	3	RPC-2.0-0.46	105.7	70	350	2	1.9	0.75	0.5	299.4	253.5	1.09
	4	RPC-2.0-0.65	105.1	70	350	2	1.9	0.75	0.5	396.7	316.42	0.95
Zhou.(2017)	5	L1	105.8	70	350	1.3	1.9	0.75	0.5	299.4	573.5	0.99
	6	L2	105.8	70	350	1.7	1.9	0.75	0.5	299.4	345.1	0.97
	7	L4	105.8	70	350	2.6	1.9	0.75	0.5	299.4	202.4	1.08
Dinh et al.(2011)	8	B27-5	44.4	203	610	3.5	2.1	1.5	0.5	0	433.41	0.98
	9	B27-6	42.8	203	610	3.5	2.1	1.5	0.5	0	421.02	0.99
	10	B27-7	37	203	610	3.5	1.6	0	-	0	160.98	1.21
Voo et al.(2010)	11	X-B1	125	50	620	3.2	0	1	0.5	1200	330	1.22
	12	X-B2	126	50	620	3.2	0	1	0.5	1200	355	1.14
	13	X-B3	135	50	620	3.2	0	1	0.5	1200	360	1.15
	14	X-B4	122	50	620	2.5	0	1	0.5	1200	456	1.01
	15	X-B5	140	50	620	3.5	0	1	0.5	1200	423	0.95
	16	X-B6	140	50	620	4.5	0	1	0.5	1200	391	0.92
	17	X-B7	122	50	620	2.5	0	1.5	0.5	1200	522	0.95
	18	X-B8	122	50	620	1.8	0	1	0.5	1200	582	1.04
Dupont et al.(2003)	19	13	40.3	200	260	1.5	1.81	0	0.5	0	210.08	1.08

	20	25	29.4	200	262	2.5	1.15	0	0.5	0	70.22	1.20
	21	28	29.4	200	260	2.5	1.81	0	0.5	0	84.76	1.17

1

2 Table 7. Summary of beam specimens (continue)

Reference	No.	Specimen	f_{cm} (MPa)	b (mm)	d (mm)	a/d	ρ (%)	V_f (%)	β_v	$P_{e,bot}$ (kN)	$V_{u,\exp}$	$V_u/V_{u,\exp}$
Voo et al.(2006)	22	SB1	161	50	600	3.3	0	2.5	0.5	0	430	0.64
	23	SB2	160	50	600	3.3	0	2.5	0.5	900	497	0.93
	24	SB3	149	50	600	3.3	0	2.5	0.5	450	428	0.82
	25	SB4	164	50	600	3.3	0	1.25	0.5	450	337	0.88
	26	SB5	171	50	600	3.3	0	2.5	0.54	450	440	0.91
	27	SB6	157	50	600	3.3	0	2.5	0.6	450	330	1.19
	28	SB7	169	50	600	3.3	0	2.5	0.52	450	400	0.97
Kwak et al.(2002)	29	FHB1-2	62.6	125	212	2	1.48	0	0.5	0	80.03	1.30
	30	FH81-3	62.6	125	212	3	1.48	0	0.5	0	67.05	0.97
	31	FHB1-4	62.6	125	212	4	1.48	0	0.5	0	52.47	0.95
	32	FHB2-2	63.8	125	212	2	1.48	0.5	0.5	0	134.89	0.98
	33	FHB2-2	30.8	125	212	2	1.48	0.5	0.5	0	107.06	0.70
	34	FHB3-2	68.6	125	212	2	1.48	0.75	0.5	0	144.16	1.07
	35	FHB2-3	63.8	125	212	3	1.48	0.5	0.5	0	81.89	1.01
	36	FHB2-3	30.8	125	212	3	1.48	0.5	0.5	0	67.58	0.75
	37	FHB3-3	68.6	125	212	3	1.48	0.75	0.5	0	90.1	1.07
	38	FHB2-4	63.8	125	212	4	1.48	0.5	0.5	0	63.87	0.99

	39	FHB2-4	30.8	125	212	4	1.48	0.5	0.5	0	53	0.79
	40	FHB3-4	68.6	125	212	4	1.48	0.75	0.5	0	72.61	1.01

Table 7. Summary of beam specimens (continue)

Reference	No.	Specimen	f_{cm} (MPa)	b (mm)	d (mm)	a/d	ρ (%)	V_f (%)	β_v	$P_{e,bot}$ (kN)	$V_{u,\exp}$	$V_u/V_{u,\exp}$
Yang.(2014)	41	FL-3a	45.2	155	362	1.5	1.75	0.8	0.9	0	424	1.09
	42	FL-3b	45.2	150	362	1.5	1.81	0.8	0.9	0	454	0.99
	43	FL-4a	45.2	175	362	2	1.55	0.8	0.9	0	340	0.97
	44	FL-4b	45.2	150	362	2	1.81	0.8	0.9	0	304	0.97
	45	FL-7a	46	150	362	3.5	1.81	0.8	0.9	0	174	1.01
	46	FL-7b	46	150	362	3.5	1.81	0.8	0.9	0	160	1.09
	47	FL-8a	49.6	152	362	2	1.78	0.8	0.9	0	310	1.03
	48	FL-8b	49.6	150	362	2	1.81	0.8	0.9	0	280	1.13
											Average	0.998
											COV	0.129

Note: f_{cm} is concrete cylinder strength; b is width of web; d is beam effective depth; a is shear span; ρ is reinforcement ratio; V_f is fiber volume; β_v is influence coefficient of steel fiber on shear load capacity; $P_{e,bot}$ is prestressing force (bottom flange).

Figure 1: Dimensions and reinforcement detailing of test specimens: (a) non-prestressed specimen, (b) prestressed specimens

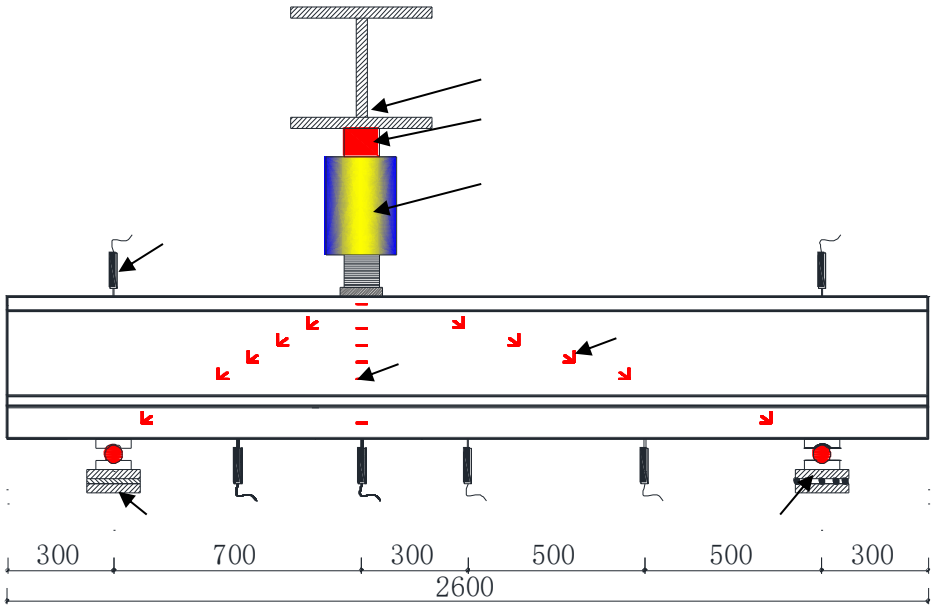

Figure 2: Overview of a specimen ready for test

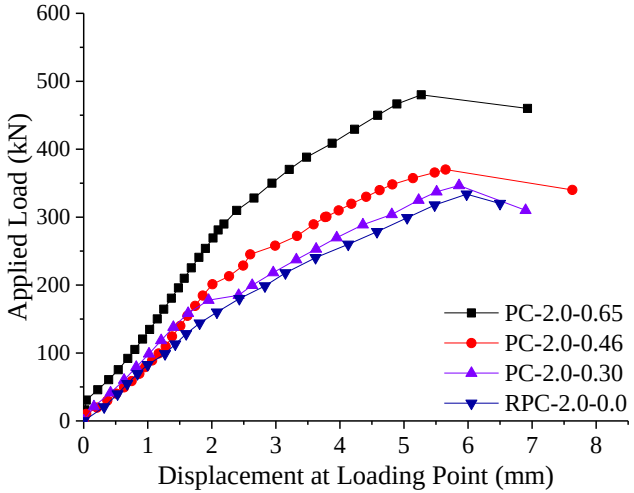

Figure 3: Load-displacement curve of test specimens

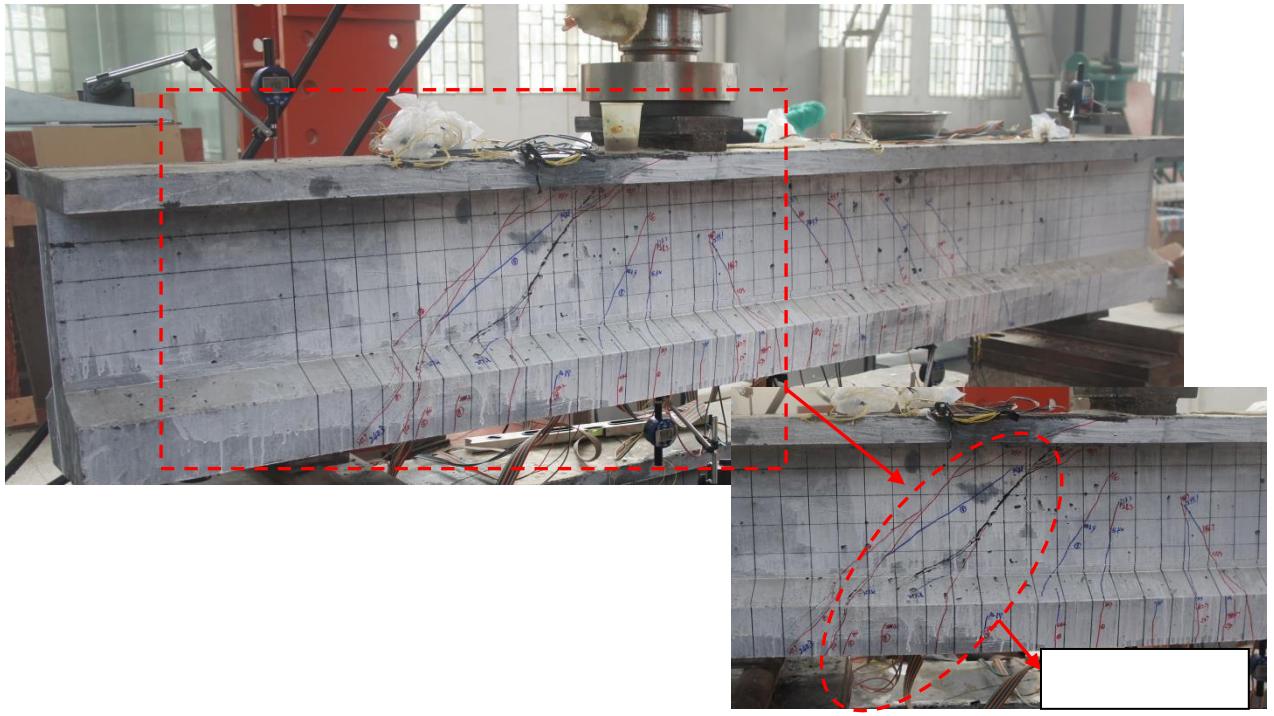

Figure 4: Failure mode of Specimen RPC-2.0-0.0

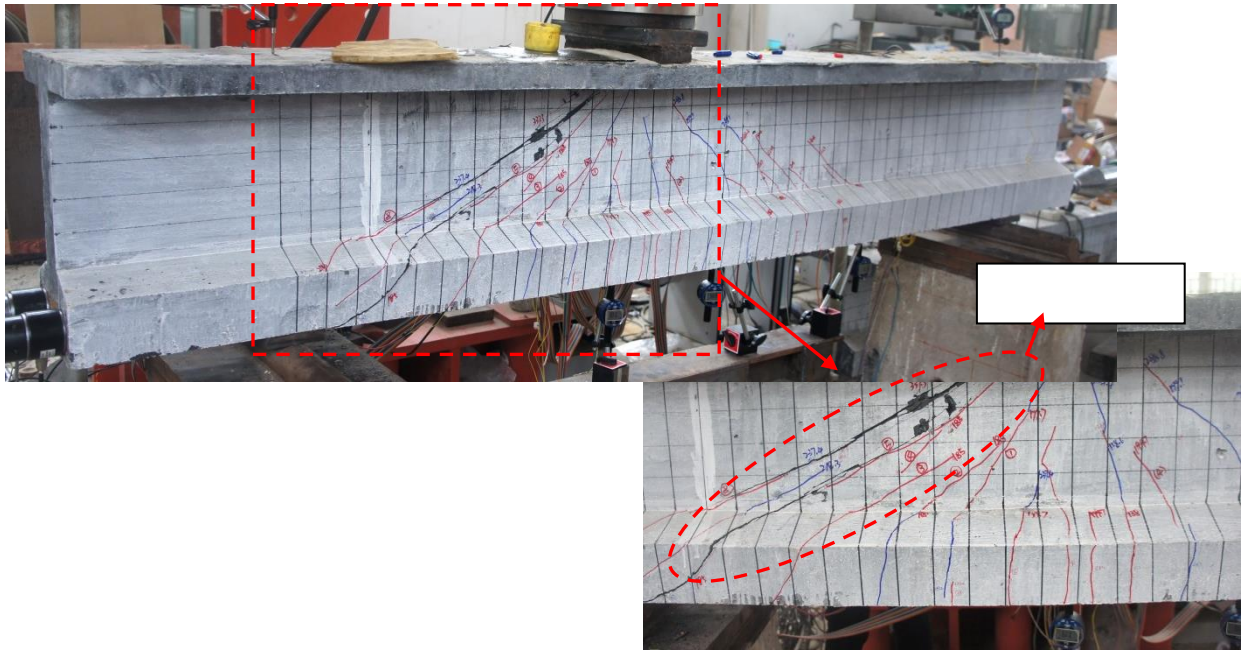

Figure 5: Failure mode of Specimen PC-2.0-0.30

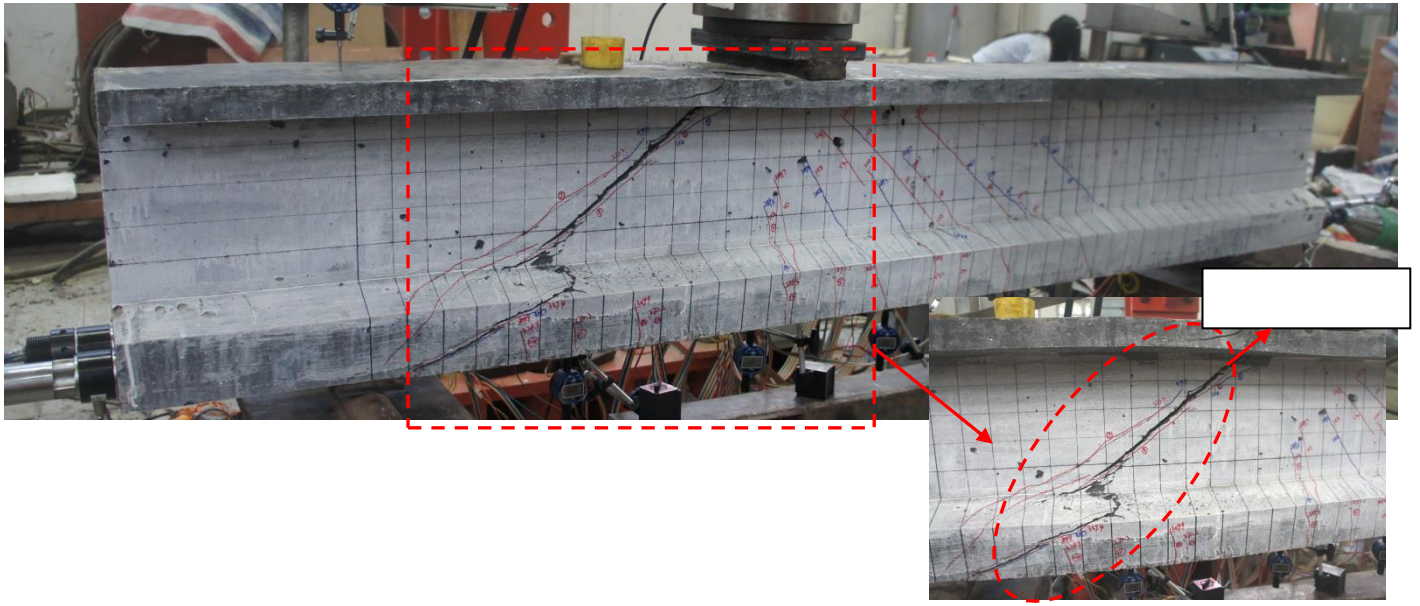

Figure 6: Failure mode of Specimen PC-2.0-0.46

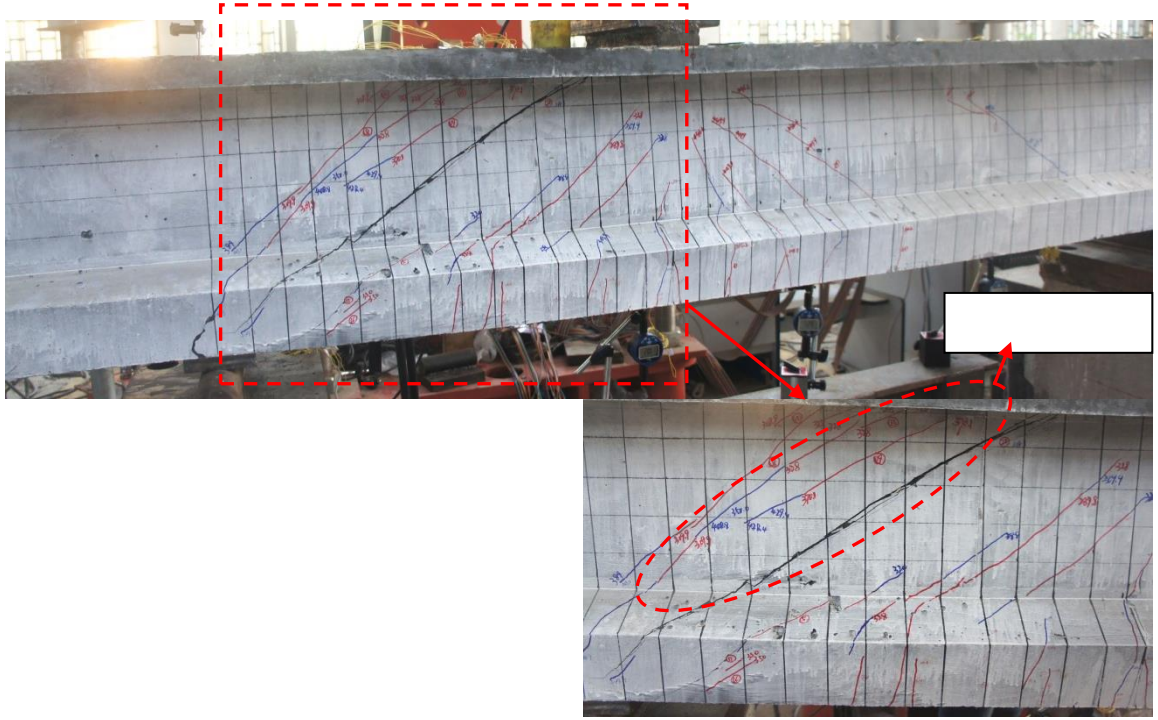

Figure 7: Failure mode of Specimen PC-2.0-0.65

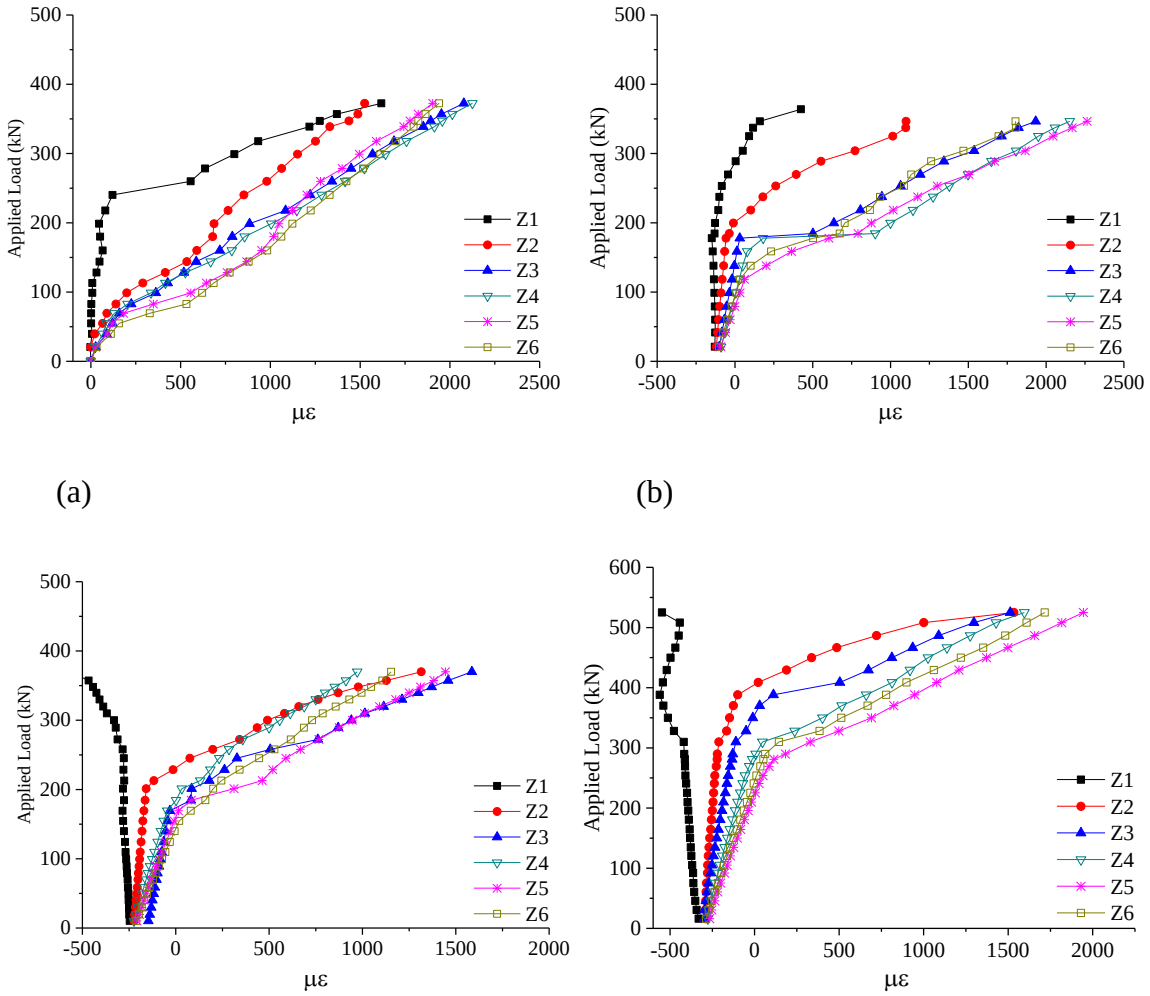

Figure 8: Strain gauge results along beam longitudinal reinforcement: (a) RPC-2.0-0.0, (b) PC-2.0-0.3 (c) PC-2.0-0.46, and (d) PC-2.0-0.65

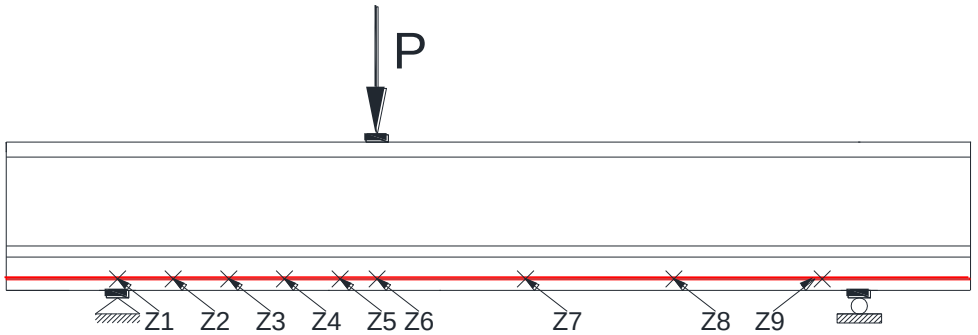

Figure 9: Locations of the strain gauges in beam longitudinal reinforcement

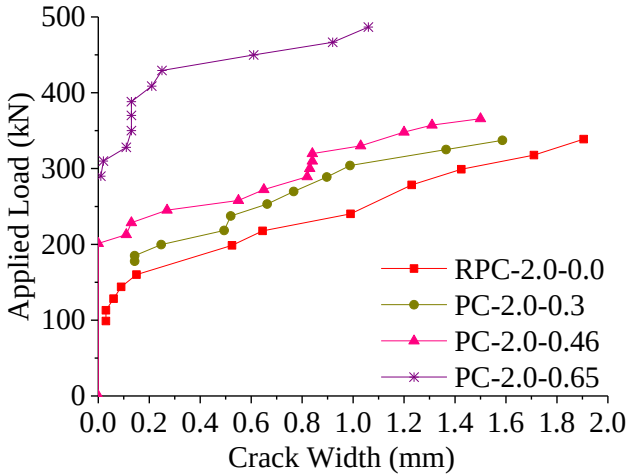

Figure 10: The relationship between applied load and crack width

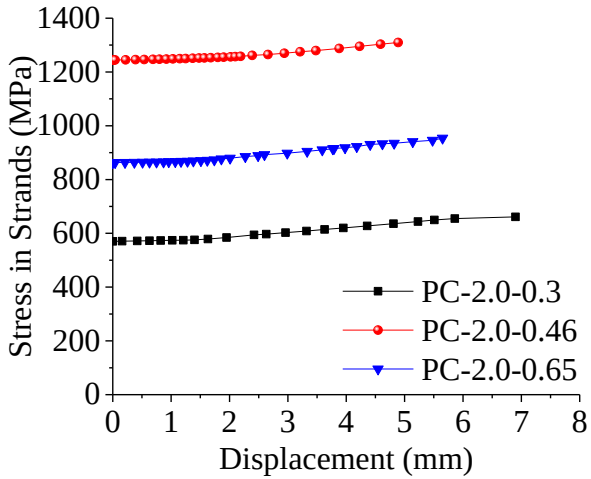

Figure 11: The relationship between stress in strands and displacement at the loading point

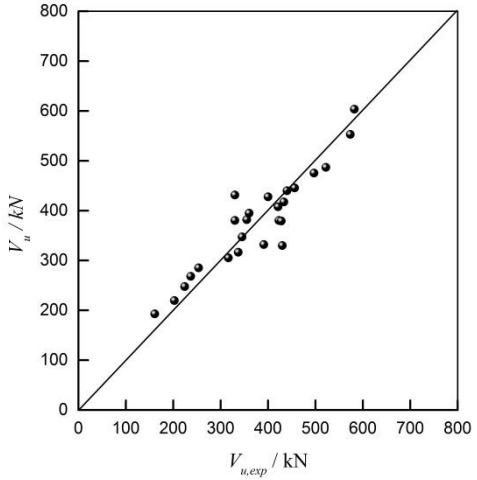

Figure 12: Comparison of the predicted and measured ultimate load